

Supernova deleptonization asymmetry: Impact on self-induced flavor conversion

Sovan Chakraborty,¹ Georg Raffelt,¹ Hans-Thomas Janka,² and Bernhard Müller³

¹*Max-Planck-Institut für Physik (Werner-Heisenberg-Institut), Föhringer Ring 6, 80805 München, Germany*

²*Max-Planck-Institut für Astrophysik, Karl-Schwarzschild-Str. 1, 85748 Garching, Germany*

³*Monash Centre for Astrophysics, School of Mathematical Sciences,
Building 28, Monash University, Victoria 3800, Australia*

(Dated: December 7, 2024)

During the accretion phase of a core-collapse supernova (SN), the deleptonization flux has recently been found to develop a global dipole pattern (LESA—Lepton Emission Self-sustained Asymmetry). The ν_e minus $\bar{\nu}_e$ flux essentially vanishes in one direction, potentially facilitating self-induced flavor conversion. On the other hand, below the stalled shock wave, self-induced flavor conversion is typically suppressed by multi-angle matter effects, preventing any impact of flavor conversion on SN explosion dynamics. In a schematic model of SN neutrino fluxes, we study the impact of modified $\bar{\nu}_e$ - ν_e flux asymmetries on collective flavor conversion. In the parameter space consisting of matter density and effective neutrino density, the region of instability with regard to self-induced flavor conversion is much larger for a vanishing lepton number flux, yet this modification does not intersect a realistic SN profile. Therefore, it appears that, even in the presence of LESA, self-induced flavor conversion remains suppressed below the shock front.

PACS numbers: 14.60.Pq, 97.60.Bw

I. INTRODUCTION

The neutrino and anti-neutrino flux spectra emitted by a core-collapse supernova (SN) significantly depend on flavor. Therefore, flavor conversion can strongly modify what neutrinos do after decoupling, notably their role in driving the explosion, determining the chemical composition and nucleosynthesis in the neutrino-driven wind after the explosion has taken off, and the expected signal in large-scale detectors from the next nearby SN. Even though neutrino mixing angles are large, in a dense matter background the eigenstates of propagation and those of interaction are very nearly the same [1]. Therefore, significant flavor conversion would only occur by the MSW effect [2, 3] at a large distance from the collapsed core because the smallness of neutrino mass differences corresponds to a relatively low resonance density.

This situation can fundamentally change when taking neutrino-neutrino refraction into account [4]. Among other effects, it can lead to self-induced flavor conversion [5, 6] even in a region of large matter density (small effective mixing angle), meaning that some spectral range of neutrino modes swap flavor with another range [7–9]. The propagation eigenmodes of the collective neutrino ensemble include run-away solutions in flavor space [10], leading to this effect. One question among many others is if self-induced flavor conversion would occur in regions below the stalled shock wave during the SN accretion phase. Flavor conversion could then modify neutrino energy deposition and impact the explosion dynamics in the framework of the neutrino-driven mechanism (Bethe-Wilson mechanism) of SN explosion.

While self-induced flavor conversion can occur at much higher density than MSW conversion, it is still suppressed by the “multi-angle matter effect” [11], although the exact conditions where conversions would occur require a

linearized stability analysis or a numerical solution of the neutrino-flavor equations of motion. Dedicated studies, using one-dimensional (1D) SN models found that the “onset radius” of self-induced flavor conversion would always lie beyond the shock front where matter densities are much smaller [12, 13]. Subsequent studies using other SN models found similar results [14, 15].

Since that time, our theoretical understanding of both self-induced flavor conversion and of flavor-dependent SN neutrino emission have both evolved. We are here especially concerned with developments having to do with spontaneous breaking of symmetries that previously were taken for granted. Axial symmetry of the neutrino radiation field around a given radial direction had been assumed in studies of collective flavor oscillations. However, a new class of run-away solutions breaks this symmetry spontaneously, allowing self-induced flavor conversion in both neutrino mass hierarchies [16–20].

The other new development is the very recent insight that SN neutrino emission in 3D models develops a global dipole pattern termed LESA for Lepton Emission Self-sustained Asymmetry [21, 22]. While the overall neutrino luminosity remains nearly spherically symmetric, the deleptonization flux (ν_e minus $\bar{\nu}_e$) develops a strong dipole pattern roughly during the first 150 ms after collapse. It survives during the entire accretion phase, irrespective of other hydrodynamical instabilities, notably the standing accretion shock instability (SASI) mode. The analyzed 3D models do not show explosions, but one would expect that this dipole pattern, which seems to be caused by the accretion flow, might disappear some 100 ms after the explosion. The LESA phenomenon implies that during the accretion phase, the deleptonization flux emerges primarily in one hemisphere. In some directions of the opposite hemisphere, it can be very small and even negative in some directions.

In an isotropic neutrino gas or in the single-angle approximation of neutrinos emitted by a SN core, a flux which is symmetric between the neutrino and anti-neutrino distributions is entirely unstable with regard to self-induced flavor conversion [24–27]. However, multi-angle effects caused by matter or by neutrinos themselves can suppress the instability. The main purpose of our study is to investigate if directions of very small ν_e - $\bar{\nu}_e$ flux asymmetry, and in density regions within the shock front, might be particularly prone to self-induced flavor conversion in either mass hierarchy.

The short answer, based on our schematic study, is that multi-angle matter suppression is the dominant effect. For the time being, it does not seem obviously wrong to ignore self-induced flavor conversion in numerical 3D studies of SN dynamics, although any such conclusion is subject to revision by more systematic studies and as our understanding of collective flavor oscillations develops.

We are here not concerned with the question what self-induced flavor oscillations would do if they were to occur, so it is enough to perform a linearized stability analysis. This is a conservative approach because even if instabilities were found, it is not assured that they would grow enough to cause significant flavor conversion.

For the moment we ignore several recent developments that may be irrelevant for our basic stability question. We ignore the “halo flux” produced by residual scattering beyond the neutrino sphere, although this flux can produce the dominant neutrino-neutrino refractive effect at large distances [28–30]. Moreover, we do not worry about the question if a quasi-stationary neutrino source would be assured to produce a quasi-stationary self-induced flavor conversion solution [16, 31]. We also ignore possible spin-flip effects caused by neutrino magnetic dipole moments [32, 33] or simply by refraction in inhomogeneous or anisotropic media [34–36], and we ignore the role of anomalous neutrino-antineutrino correlations [37–39]. We finally ignore speculations about modified equations of motion caused by wave-packet separation [40].

We begin in Sec. II with a brief account of the linear stability analysis used in our study, followed in Sec. III by a description of the assumed schematic neutrino flux characteristics. We then turn to our actual stability analysis in Sec. IV before concluding in Sec. V.

II. FLAVOR STABILITY CONDITIONS

To set up our stability analysis, we follow Ref. [16], although we will slightly adapt some normalizations. The flavor-dependent neutrino fluxes emerging from a SN core depend, at a given radius r , on energy E , zenith angle Θ relative to the radial direction, and azimuth angle φ in a tangential coordinate system. We assume neutrino free streaming beyond some reference radius R which we call “neutrino sphere”, although it need not coincide with the physical neutrino decoupling region. It is then convenient to describe the zenith direction with a fixed label $u =$

$\sin^2 \Theta_R$ where Θ_R is the zenith angle at radius R .

We combine the flavor-dependent fluxes into a matrix $F_{r,E,u,\varphi}$ which depends on the variables given as indices. (We denote matrices in flavor space with capital sans-serif letters.) The diagonal entries are the ordinary neutrino fluxes F_α for species α , expressed as 4π equivalent fluxes. The off-diagonal elements contain coherence information caused by flavor oscillations. We use negative energies to denote anti-neutrinos and in this case there is also a sign change for the fluxes themselves. Assuming the solution is stationary and varies at most slowly as a function of global direction, the radial variation of the flux matrix is given by the equation of motion [10, 16]

$$i\partial_r F_{E,u,\varphi} = [H_{E,u,\varphi}, F_{E,u,\varphi}], \quad (1)$$

where we have suppressed the index r on all quantities. The Hamiltonian matrix governing the evolution is [16]

$$H_{E,u,\varphi} = \frac{1}{v_u} \left(\frac{M^2}{2E} + \sqrt{2} G_F N_\ell \right) + \frac{\sqrt{2} G_F}{4\pi r^2} \int d\Gamma' \left(\frac{1 - v_u v_{u'} - \beta_u \cdot \beta_{u'}}{v_u v_{u'}} \right) F', \quad (2)$$

where M^2 is the neutrino mass-squared matrix. The factor v_u^{-1} arises from projecting the oscillations on the radial direction. This factor causes the crucial multi-angle matter suppression: neutrinos traveling in different directions accrue different phases along the radial direction. The matter term, assumed to be isotropic, is given by the matrix N_ℓ of net charged-lepton densities which is diagonal in the weak-interaction basis. The third term represents neutrino-neutrino refraction and is given by the phase-space integral $\int d\Gamma' = \int_{-\infty}^{+\infty} dE' \int_0^1 du' \int_0^{2\pi} d\varphi'$ where the flux matrix F' is understood as $F_{E',u',\varphi'}$ at radius r . The radial velocity of a given mode u is $v_u = (1 - uR^2/r^2)^{1/2}$ [27]. The transverse velocity β depends on the azimuth angle φ . One finds $|\beta_u| = \sqrt{u} R/r$ and $\beta_u \cdot \beta_{u'} = \sqrt{uu'} (R/r)^2 \cos(\varphi - \varphi')$ [16].

We restrict our stability analysis to a two-flavor system and express the flux matrices in the form

$$F = \frac{\text{Tr } F}{2} + \frac{F_{\nu_e}^R - F_{\nu_x}^R}{2} \begin{pmatrix} s & S \\ S^* & -s \end{pmatrix}, \quad (3)$$

where s is real, S complex, and $s^2 + |S|^2 = 1$. The fluxes are set at the neutrino-sphere radius R where $s = 1$ and $S = 0$. Since the overall neutrino flux is conserved, the trace term is conserved and drops out of the commutator equation. We further change the energy variable E to the frequency variable $\omega = \Delta m_{\text{atm}}^2 / 2E$ which is more convenient in the flavor oscillation context.

We finally normalize all fluxes to the $\bar{\nu}_e$ flux at the neutrino sphere and define the spectrum

$$g = \frac{1}{F_{\bar{\nu}_e}} \begin{cases} F_{\nu_e} - F_{\nu_x} & \text{for } \omega > 0 \\ F_{\bar{\nu}_x} - F_{\bar{\nu}_e} & \text{for } \omega < 0 \end{cases} \quad (4)$$

where g and all fluxes depend on ω , u , and φ . With the spectrum thus normalized, we define the asymmetry parameter as

$$\epsilon = \int_{-\infty}^{+\infty} d\Gamma g(\omega, u, \varphi), \quad (5)$$

where $\int d\Gamma = \int_{-\infty}^{+\infty} d\omega \int_0^1 du \int_0^{2\pi} d\varphi$. This definition of g and thus of ϵ is somewhat different from previous studies. Flavor oscillations can only change the difference between flavor-dependent spectra, and so it often was useful to use the net flux $F_{\bar{\nu}_e} - F_{\nu_e}$ as a baseline flux. However, in the maximal lepton flux direction of our 3D models, this difference becomes very small or even vanishes and thus can not be used to normalize other fluxes.

We finally linearize the equations of motion in two ways. We assume $|S| \ll 1$ as we want to discover modes of exponential growth in S , implying $s = 1$ to linear order. Furthermore, we use the large-distance approximation, $r \gg R$, leading to [16],

$$\begin{aligned} i\partial_r S &= [\omega + u(\lambda + \epsilon\mu)]S \\ &- \mu \int d\Gamma' [u + u' - 2\sqrt{uu'} \cos(\varphi - \varphi')] g' S', \end{aligned} \quad (6)$$

where S depends on ω , u and φ , whereas S' and g' depend on ω' , u' and φ' . The effective multi-angle strength of the neutrino-neutrino and neutrino-matter interaction are described by the parameters

$$\mu = \frac{\sqrt{2} G_F F_{\bar{\nu}_e}^R R^2}{4\pi r^2}, \quad (7)$$

$$\lambda = \sqrt{2} G_F n_e \frac{R^2}{2r^2}. \quad (8)$$

We then seek eigenvalues $\Omega = \gamma + i\kappa$ for solutions of the form $S(r, \omega, u, \varphi) = Q_{\omega, u, \varphi} e^{-i\Omega r}$, where a non-vanishing imaginary part κ reflects unstable solutions.

We finally assume axially symmetric neutrino emission, implying $g(\omega, u, \varphi) \rightarrow g(\omega, u)/2\pi$, but not necessarily an axially symmetric solution. In this case one finds the eigenvalue equation

$$(I_1 - 1)^2 = I_0 I_2 \quad \text{or} \quad I_1 = -1, \quad (9)$$

where

$$I_n = \mu \int d\omega du \frac{u^n g(\omega, u)}{\omega + u(\lambda + \epsilon\mu) - \Omega}. \quad (10)$$

The first condition leads to axially symmetric solutions in inverted hierarchy (IH) of neutrino masses and in normal hierarchy (NH). The second equation leads to a solution which breaks axial symmetry and exists only in NH.

As a simple example we consider a single-energy and single zenith angle spectrum of the form

$$g(\omega, u) = \left[(1 + \epsilon)\delta(\omega - \omega_0) - \delta(\omega + \omega_0) \right] \delta\left(u - \frac{1}{2}\right) \quad (11)$$

and we define $\Omega' = \Omega - (\lambda + \epsilon\mu)/2$. All integrals can be done explicitly and one finds the conditions $I = 1$ or $I = -2$ where

$$I = \mu \int d\omega \frac{g(\omega)}{\omega - \Omega'} = \mu \left(\frac{1 + \epsilon}{\omega_0 - \Omega'} - \frac{1}{-\omega_0 - \Omega'} \right). \quad (12)$$

The quadratic equation resulting from the first condition has the solution

$$\Omega = \frac{1}{2} \left(\lambda \pm \sqrt{(2\omega_0 - \epsilon\mu)^2 - 8\omega_0\mu} \right). \quad (13)$$

To have an imaginary part, the argument of the square-root must be negative. This can only happen if $\omega_0\mu > 0$, corresponding in our conventions to IH, and is the usual bimodal instability. The solution has an imaginary part and thus a run-away solution for μ between the limits $2\omega_0/(\sqrt{1 + \epsilon} \pm 1)^2$. In particular, for a vanishing asymmetry, $\epsilon = 0$, the system is unstable for $\omega_0 < \mu < \infty$, i.e., it is unstable for all but the smallest neutrino densities. The other condition produces the solution

$$\Omega = \frac{1}{4} \left(2\lambda + 3\epsilon\mu \pm \sqrt{(4\omega_0 + \epsilon\mu)^2 + 16\omega_0\mu} \right), \quad (14)$$

which can have an imaginary part only if $\omega_0\mu < 0$, corresponding to NH. This is the solution breaking axial symmetry, previously termed the multi-azimuth-angle (MAA) solution. It is unstable on the $|\mu|$ range between $4\omega_0/(\sqrt{1 + \epsilon} \pm 1)^2$. For vanishing asymmetry this would be the unstable range $2\omega_0 < |\mu| < \infty$.

This exercise reveals that, in both hierarchies and in the single-angle case, the system will be stable for μ above some value depending on ω_0 and on the asymmetry. This high-density stable solution was called the ‘‘synchronized regime’’ or ‘‘sleeping top regime,’’ whereas for neutrino densities below some critical value, the instability sets in. For a vanishing asymmetry, this regime would not exist and the system would be unstable for any density except the very lowest ones. It is this observation which raises the question of what happens in the low-asymmetry directions in the LESA context.

The short answer is that it is multi-angle effects alone [12, 13, 20] which prevent the instability in this case. Therefore, we need to perform a multi-angle stability analysis. It was noted previously that the MAA solution is more difficult to suppress by multi-angle effects. Therefore, we will henceforth focus on this conservative case to perform a stability analysis, i.e., we consider the second condition in Eq. (9). Explicitly, then, we will study the condition

$$\int d\omega du \frac{u g(\omega, u)}{\omega + u(\lambda + \epsilon\mu) - \Omega} = -\frac{1}{\mu}, \quad (15)$$

for the schematic SN model presently described.

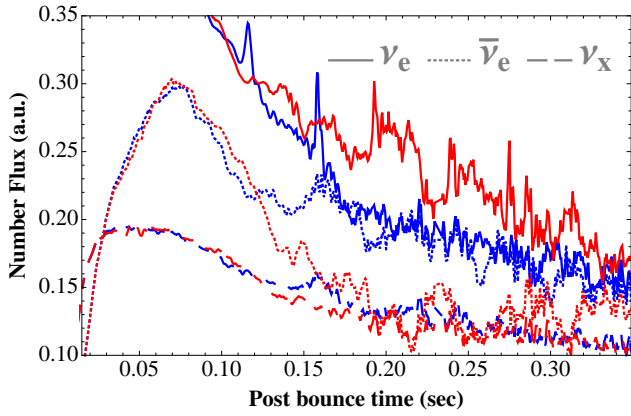


FIG. 1: Evolution of the flavor-dependent neutrino number fluxes in the directions of minimal (blue lines) and maximal (red lines) lepton-number flux. The ν_x flux (representing any of ν_μ , $\bar{\nu}_\mu$, ν_τ and $\bar{\nu}_\tau$), shown in dashed line, is similar in both directions. The $\bar{\nu}_e$ flux (dotted) develops a large asymmetry at around 150 ms p.b. In the direction of minimal lepton number flux, the $\bar{\nu}_e$ flux is as large as the ν_e flux, in the opposite direction it is as small as the ν_x flux.

III. SCHEMATIC LESA MODEL FOR SUPERNOVA NEUTRINO FLUXES

We construct a schematic model of SN neutrino fluxes motivated by the 3D models that have led to the identification of the LESA phenomenon [21, 22]. Specifically, we use the model with $11.2 M_\odot$ progenitor mass as a benchmark for our study. During the accretion phase, this model shows large-scale convective overturn, but it does not develop the standing accretion shock instability (SASI), in contrast to the models with larger progenitor masses. After about 150 ms post bounce (p.b.), this and the other models develop a large-scale anisotropy of lepton-number emission.

We illustrate this behavior in Fig. 1 with the flavor-dependent neutrino number fluxes in two opposite directions, roughly corresponding to the directions of maximal (red curves) and minimal (blue curves) lepton-number flux, respectively. The ν_e , $\bar{\nu}_e$ and ν_x flavors are distinguished by continuous, dotted and dashed lines, respectively. We follow this color code in all the figures. The ν_x fluxes in the two opposite directions are similar. However, in the minimum direction, the $\bar{\nu}_e$ flux is similar to the ν_e flux, corresponding to a small lepton asymmetry. In the maximum direction, the $\bar{\nu}_e$ and ν_x fluxes are similar and much smaller than the ν_e flux. We note that these fluxes are not ray-by-ray fluxes, but are extracted from the simulation in a post-processing step that takes the lateral propagation of neutrinos into account in an approximative fashion to obtain direction-dependent fluxes far away from the neutrinosphere [22, 23]. More details on the angular distribution of the number and energy fluxes and their evolution are given in Refs. [21, 22].

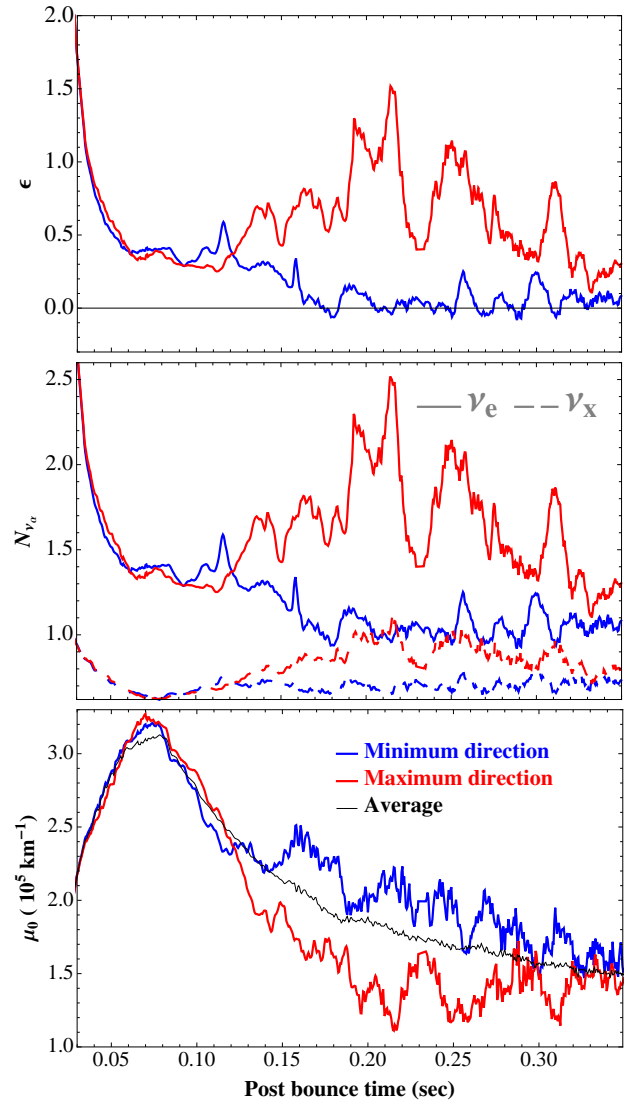


FIG. 2: Physical characteristics of our benchmark SN model in the minimum and maximum lepton-flux directions. *Top*: Asymmetry parameter ϵ of the lepton-number flux as defined in Eq. (16). *Middle*: ν_e and ν_x flux relative to $\bar{\nu}_e$ flux. *Bottom*: Effective neutrino-neutrino interaction strength μ_0 at the neutrino sphere.

We will usually express flavor-dependent fluxes relative to the $\bar{\nu}_e$ flux. In particular, we express the lepton-number flux in terms of the flux asymmetry parameter

$$\epsilon = \frac{F_{\nu_e} - F_{\bar{\nu}_e}}{F_{\bar{\nu}_e}} \quad (16)$$

in agreement with our earlier definition in Eq. (5). We show the evolution of ϵ in Fig. 2 for the two extreme directions. Once more we recognize that the lepton-number flux in the minimal direction nearly vanishes or even becomes slightly negative after about 150 ms p.b.

The middle panel of Fig. 2 shows the time variation of the ν_e and ν_x flux relative to the $\bar{\nu}_e$ flux ($N_{\nu_\alpha} = F_{\nu_\alpha}/F_{\bar{\nu}_e}$)

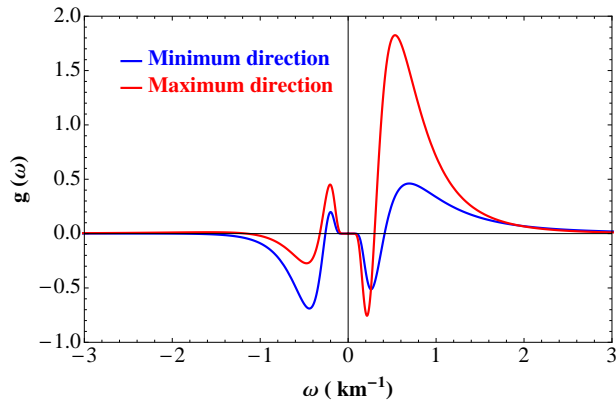


FIG. 3: Neutrino spectrum for our model (210 ms p.b.) as defined in Eq. (4) in terms of the vacuum oscillation frequency $\omega = \Delta m^2/2E$, where negative ω is for antineutrinos. Blue curve: direction of minimum lepton-number flux. Red curve: maximum direction.

for both extreme directions. In both directions N_{ν_x} can be reasonably approximated as constant when compared with the much larger variations in N_{ν_e} .

Finally, another crucial parameter is the effective neutrino-neutrino interaction strength defined in Eq. (7). The first factor is essentially the weak potential that would be caused by an isotropic neutrino gas at radius r , whereas the second factor accounts for neutrinos being ever more collinear with increasing distance, reducing the effective interaction strength. Overall one obtains the usual r^{-4} variation of the effective interaction potential. Once more, in previous studies this parameter had been normalized to the $\bar{\nu}_e$ - $\bar{\nu}_x$ flux difference whereas here we use the $\bar{\nu}_e$ flux for normalization as explained earlier. We show $\mu_0 = \mu(R)$ as a function of time for our model in the bottom panel of Fig. 2. A typical value is a few 10^5 km^{-1} . There is a large variation of μ between the two extreme lepton-flux directions. We also plot the 4π average of μ_0 which shows a smooth variation compared to the two extreme directions.

For the purpose of flavor oscillations, a natural parameter to characterize the neutrino energy is the vacuum oscillation frequency which in our two-flavor scenario is $\omega = \Delta m^2/2E$. Moreover, as explained earlier, we use negative ω values to describe anti-neutrinos. Ignoring for the moment angular variables, we show an example for the effective neutrino spectrum $g(\omega)$ in Fig. 3 for a snapshot of our model at 210 ms p.b.. In the direction of minimal lepton-number flux (blue curve), the spectrum is mostly positive for positive ω and mostly negative for negative ω and the overall integral nearly vanishes, corresponding to $\epsilon \sim 0$. In the opposite direction (red curve), the spectrum essentially vanishes for negative ω , corresponding to the spectra of $\bar{\nu}_e$ and $\bar{\nu}_x$ being almost identical. The flavor-dependent spectra as functions of energy corresponding to this case are given in Fig. 14 of Ref. [21].

We notice that the frequency spectrum $g(\omega)$ is domi-

nated by a relatively narrow range around one positive and one negative frequency. To simplify our discussion even further, we therefore adopt a very schematic representation of this situation in terms of the “single energy” spectrum

$$g(\omega) = \frac{F_{\nu_e} - F_{\nu_x}}{F_{\bar{\nu}_e}} \delta(\omega - \omega_0) - \frac{F_{\bar{\nu}_e} - F_{\bar{\nu}_x}}{F_{\bar{\nu}_e}} \delta(\omega + \omega_0), \quad (17)$$

where the contributions arise at $\omega = \pm\omega_0$. Specifically we use $E = 12 \text{ MeV}$ as our single energy, corresponding to $\omega_0 = \Delta m_{\text{atm}}^2/2E = 0.51 \text{ km}^{-1}$.

For the zenith-angle distribution we use the variable $u = \sin^2 \Theta_R$ with the emission angle Θ_R at our reference radius R which we take to be 35 km. Blackbody-like isotropic emission at the neutrino sphere would correspond to a flat distribution on the interval $0 \leq u \leq 1$. However, the neutrino distribution tends to be more forward biased in the decoupling region. We still assume a flat distribution on an interval $0 \leq u \leq u_1$ where $u_1 < 1$. The average neutrino-neutrino interaction strength is larger for a broader zenith-angle distribution, or conversely, the multi-angle matter suppression is more effective for a more forward-peaked distribution [20, 41]. In our stability analysis we will use both the extreme assumption of $u_1 = 1$, which exaggerates the effective strength of neutrino-neutrino interactions, and a more realistic forward-peaked value of $u_1 = 0.5$.

In summary, inspired by the $11.2 M_\odot$ model of Ref. [21], we will use the following parameters for our stability analysis. We use a single-energy spectrum with energy 12 MeV for all species, corresponding to a vacuum oscillation frequency of $\omega_0 = 0.51 \text{ km}^{-1}$. We will use a value $\mu_0 = 2 \times 10^5 \text{ km}^{-1}$ for the effective neutrino-neutrino strength at the neutrino sphere which is at the upper end of what is seen during the LESA phase after around 150 ms p.b. and which is conservative in that it provides a relatively strong neutrino-neutrino effect. For the relative ν_x flux we use the fixed values 0.7 and 0.95 in the minimum and maximum lepton-number flux directions, respectively. The zenith-angle distribution at the neutrino sphere is taken to be blackbody-like (isotropic in one half-space) as the most extreme case, or forward peaked with a top-hat distribution on $0 \leq u \leq 0.5$. The most important parameter is the asymmetry ϵ . In the minimum lepton flux direction we will use values $\epsilon_{\text{min}} = -0.05, 0, 0.05$, and 0.2. In the opposite direction we will use $\epsilon_{\text{max}} = 0.5, 1$, and 1.5.

IV. STABILITY ANALYSIS

It remains to actually perform the stability analysis for the schematic model described in the previous section. As a formal criterion for instability we adopt $\kappa > 0.01 \text{ km}^{-1}$ where on the available distance scale a putative instability could grow significantly. We therefore solve Eq. (15) and determine the contour $\kappa = 0.01 \text{ km}^{-1}$ in the plane consisting of the effective neutrino-neutrino

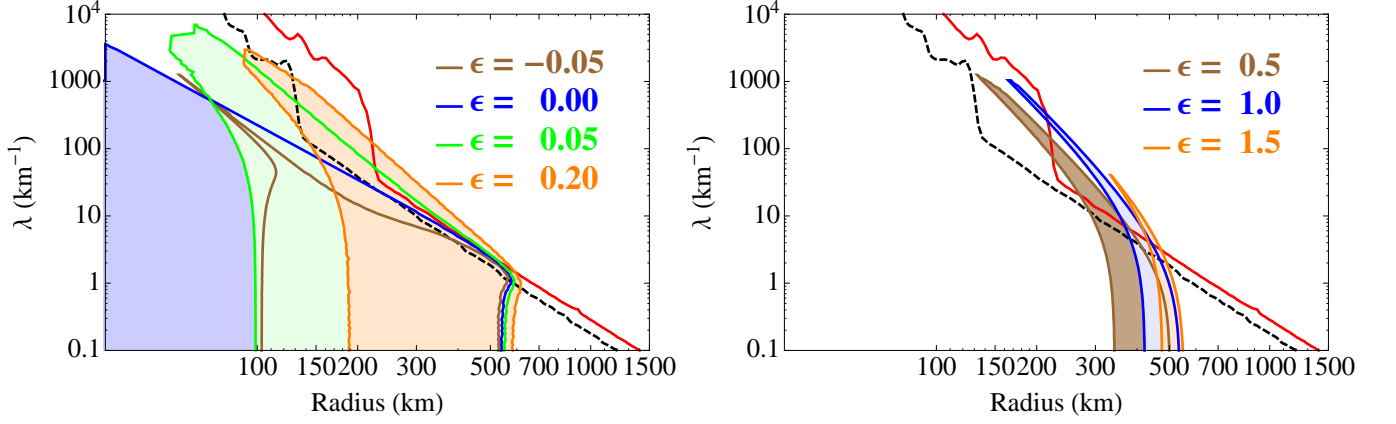


FIG. 4: Instability region ($\kappa > 0.01 \text{ km}^{-1}$) for the uniform zenith distribution ($0 \leq u \leq 1$). Representative SN density profiles at 150 ms p.b. and 350 ms p.b are shown by continuous red and dashed black curves, respectively. *Left*: Direction of minimal lepton flux with $\epsilon = -0.05, 0.0, 0.05$, and 0.1 as indicated. *Right*: Direction of maximal lepton flux with $\epsilon = 0.5, 1.0$ and 1.5 .

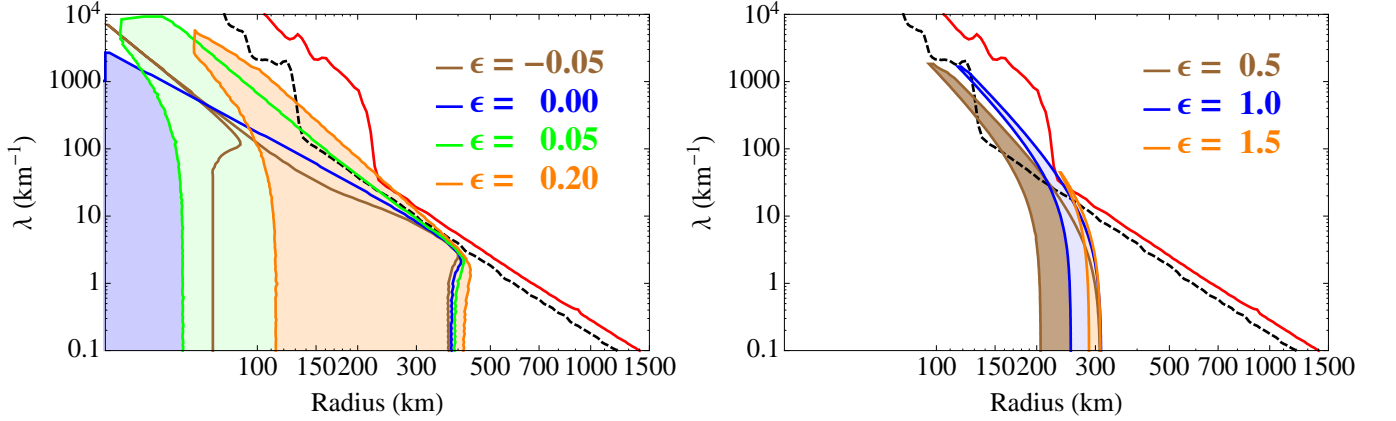


FIG. 5: Same as Fig. 4 for a forward peaked angular distribution ($0 \leq u \leq 0.5$).

interaction strength μ and the interaction strength λ for the multi-angle matter effect. Actually, instead of μ we will use the distance r as one of the parameters by virtue of $\mu = \mu_0 (R/r)^4$ with $R = 35 \text{ km}$ and $\mu_0 = 2 \times 10^5 \text{ km}^{-1}$. In this way we show the instability region in the parameter space spanned by r and λ , the latter being proportional to the net electron density. In this parameter space we can thus include effectively the SN electron-density profile, allowing a simple visual inspection of the instability region vs. actual SN density profile.

As an extreme case, exaggerating the effect of neutrino-neutrino interaction and thus a possible self-induced instability, we assume a uniform zenith-angle distribution ($0 \leq u \leq 1$), corresponding to blackbody-like isotropic emission at radius R .

Figure 4 shows the instability region ($\kappa = 0.01 \text{ km}^{-1}$) in the parameter space consisting of λ and r . In the left panel, we consider our direction of small lepton-number flux and use asymmetry values $\epsilon = -0.05, 0.00, 0.05$, and 0.20 . This figure illustrates our main finding: Small values of ϵ strongly enlarge the instability region, however

in the direction towards the lower left of the plot. This corresponds to regions of small matter density and large neutrino density where the multi-angle matter effect is small, the neutrino-neutrino effect is large.

The right panel shows the direction of large lepton number flux which we model with the asymmetry values $\epsilon = 0.5, 1.0$, and 1.5 . The instability region is now a narrow sliver and slightly moves to the right (small neutrino densities) for increasing asymmetry.

In both panels we superpose typical SN density profiles, taken from the numerical simulation of the $11.2 M_\odot$ at 150 ms and 350 ms p.b. The dramatic density drops at the shock-wave radius of around 220 km and 130 km are conspicuous. In these examples, the density in the region below the shock front is large enough to suppress the instability by multi-angle matter effects. In most of these examples, however, the neutrino flux would be unstable to self-induced flavor conversion directly outside of the shock front.

Next we repeat this exercise with a zenith-angle distribution that is somewhat more realistic, i.e., forward

peaked in the decoupling region. We now use $0 \leq u \leq 0.5$, effectively decreasing the neutrino-neutrino interaction strength. As expected (see Fig. 5), the instability regions are shifted downward and somewhat to the left, i.e., a smaller matter density resulting in stronger suppression of the self-induced flavor conversions.

In the case of 150 ms p.b. example, the SN density profile typically does not intersect the instability region, i.e., even outside of the shock front there would not be any self-induced flavor conversion. In the few cases it barely crosses the instability, the crossing widths are extremely small. The instabilities will not have enough time to grow to any effective flavor conversion.

On the other hand, the SN density profile for 350 ms p.b. shows larger intersections with the instability region. In this case the shock radius has decreased to 130 km compared to about 200 km at 150 ms, signaling that the SN model was unsuccessful to develop an explosion up to this stage. In some simulations, where the explosion was triggered artificially, the shock front did not decrease to such small radii and therefore intersections did not occur [20]. However, there is no reason to expect that the shock must monotonically expand, and two-dimensional simulations have suggested that explosions by the delayed SN mechanism might indeed occur after transient phases of shock recession [42–44]. In particular in these cases it may be very important to more closely investigate the influence of neutrino oscillations on the further shock evolution and the detectable neutrino emission.

Large intersections, potentially even behind the shock front, might also occur in higher-mass progenitors where the shock-front radius oscillates wildly due to the SASI mode and the shock surface can be highly deformed in combination with largely non-spherical and time-variable neutrino luminosities. In the 20 and 27 M_\odot LESA models studied in Ref. [21] the shock-front radius decreases during the first few 100 ms to subsequently expand (but without initiating SN explosions in those models). Such situations might lead to large crossings of density profiles and instability regions and should be explored in future work. Our present analysis clears the background for such star and SN dynamics dependent studies because it shows that the asymmetric lepton emission associated with LESA has important quantitative consequences, although it does not radically change the picture of flavor instabilities. In particular, an extremely small lepton asymmetry does not per se ensure flavor conversions, but interesting scenarios could be connected to the shock deformation and unsteady shock propagation in special SN conditions.

V. CONCLUSIONS

Motivated by the LESA effect, we have studied a very schematic example of the impact of an unusually small lepton-number flux on the interplay between self-induced neutrino flavor conversion and its multi-angle matter sup-

pression. The instability regions are strongly enlarged into regions of small matter density and large neutrino density as perhaps expected. However, in stability plots of the type shown in our Figs. 4 and 5 this is the direction away from a typical SN density profile. Lowering the lepton-number flux by itself does not have the effect of leading to self-induced flavor conversion in regions below the shock front.

The main point of our simple study was to explore the direction of the effect of lowering the lepton-number flux. According to our results, it is not obviously reckless to ignore self-induced flavor conversion for studying the SN explosion dynamics. Of course, flavor conversion will be important outside of the shock front, certainly at large distances by the MSW effect, and perhaps in some cases directly outside of the shock front by self-induced flavor conversion. Such effects would be important for the interpretation of the neutrino signal from the next nearby SN, but would not directly affect the explosion dynamics.

Our stability analysis was rather schematic with the purpose of exploring the general direction of what an unusually small lepton-number flux caused by the LESA effect would do. In principle, of course, in any given SN simulation one could perform a posterior stability analysis, based on the numerical neutrino radiation field and density profile, to verify that it was justified to ignore flavor conversion. In 3D simulations performed in Garching, this stability analysis would have to be performed for each of the angular bins. In the ray-by-ray technique for neutrino transport employed in the Garching code, the neutrino transport in any such angular bin effectively represents a cone in which the neutrino radiation field is treated as part of a spherically symmetric distribution. In this sense our approach to self-induced flavor conversion, assuming a purely radial variation of all properties of the neutrino radiation field, would be consistent with the ray-by-ray approach. In principle, then, one could develop a numerical tool that could flag possible flavor instabilities as the numerical simulation progresses. Of course, should cases be found where flavor conversion below the shock front occurs after all, a completely new challenge has to be faced in SN modeling.

We stress, however, that not finding flavor-conversion instabilities in this approach does not necessarily prove that none exist. As explained in the introduction, we have ignored a number of new issues that have emerged in the recent literature on neutrino-neutrino refractive effects. These topics should be sorted out before worrying further about self-induced flavor conversion in practical SN simulations. In particular, the multi-angle matter effect which provides the stabilizing ingredient in the present context relies on the assumption that the neutrino radiation field and its flavor properties can vary only along the radial direction. This is an imposed symmetry assumption which can hide unstable solutions that might exist otherwise. Likewise, the assumption of a purely stationary solution, allowing us to treat the problem in the form of an ordinary (rather than partial) dif-

ferential equation has never been strictly justified.

The core-collapse SN explosion mechanism is one of the few physical phenomena where neutrinos play a dominant dynamical role and where the flavor dependence of the fluxes matters. Yet flavor conversion, in spite of large mixing angles, does not seem to figure at all for SN dynamics due to matter suppression of flavor oscillations, i.e., because in dense matter, propagation and interaction eigenstates are almost the same. However, a final verdict on the role of active-active flavor conversion for SN dynamics requires more theoretical work to fully appreciate the role of possible flavor instabilities in the interacting neutrino field.

Acknowledgments

This work was partly supported by the Deutsche Forschungsgemeinschaft under Grant No. EXC-153 (Cluster of Excellence Origin and Structure of the Universe) and by the European Union under Grant No. PITN-GA-2011-289442 (FP7 Initial Training Network Invisibles). S.C. acknowledges support from the European Union through a Marie Curie Fellowship, Grant No. PIIF-GA-2011-299861.

-
- [1] L. Wolfenstein, Phys. Rev. D **17**, 2369 (1978).
 - [2] S. P. Mikheev and A. Y. Smirnov, Sov. J. Nucl. Phys. **42**, 913 (1985) [Yad. Fiz. **42**, 1441 (1985)]; Sov. Phys. JETP **64**, 4 (1986) [Zh. Eksp. Teor. Fiz. **91**, 7 (1986)].
 - [3] A. S. Dighe and A. Y. Smirnov, Phys. Rev. D **62**, 033007 (2000) [hep-ph/9907423].
 - [4] J. Pantaleone, Phys. Lett. B **287**, 128 (1992).
 - [5] V. A. Kostelecký and S. Samuel, Phys. Lett. B **318**, 127 (1993).
 - [6] S. Samuel, Phys. Rev. D **53**, 5382 (1996) [hep-ph/9604341].
 - [7] H. Duan, G. M. Fuller and Y.-Z. Qian, Phys. Rev. D **74**, 123004 (2006) [astro-ph/0511275].
 - [8] H. Duan, G. M. Fuller, J. Carlson and Y.-Z. Qian, Phys. Rev. D **74**, 105014 (2006) [astro-ph/0606616].
 - [9] H. Duan, G. M. Fuller and Y.-Z. Qian, Annu. Rev. Nucl. Part. Sci. **60**, 569 (2010) [arXiv:1001.2799].
 - [10] A. Banerjee, A. Dighe and G. Raffelt, Phys. Rev. D **84**, 053013 (2011) [arXiv:1107.2308].
 - [11] A. Esteban-Pretel, A. Mirizzi, S. Pastor, R. Tomàs, G. G. Raffelt, P. D. Serpico and G. Sigl, Phys. Rev. D **78**, 085012 (2008) [arXiv:0807.0659].
 - [12] S. Chakraborty, T. Fischer, A. Mirizzi, N. Saviano and R. Tomàs, Phys. Rev. Lett. **107**, 151101 (2011) [arXiv:1104.4031].
 - [13] S. Chakraborty, T. Fischer, A. Mirizzi, N. Saviano and R. Tomàs, Phys. Rev. D **84**, 025002 (2011) [arXiv:1105.1130].
 - [14] B. Dasgupta, E. P. O'Connor and C. D. Ott, Phys. Rev. D **85**, 065008 (2012) [arXiv:1106.1167].
 - [15] S. Sarikas, G. G. Raffelt, L. Hudepohl and H. T. Janka, Phys. Rev. Lett. **108**, 061101 (2012) [arXiv:1109.3601].
 - [16] G. Raffelt, S. Sarikas and D. de Sousa Seixas, Phys. Rev. Lett. **111**, 091101 (2013) [arXiv:1305.7140].
 - [17] G. Raffelt and D. de S. Seixas, Phys. Rev. D **88**, 045031 (2013) [arXiv:1307.7625].
 - [18] A. Mirizzi, Phys. Rev. D **88**, 073004 (2013) [arXiv:1308.1402].
 - [19] S. Chakraborty and A. Mirizzi, Phys. Rev. D **90**, 033004 (2014) [arXiv:1308.5255].
 - [20] S. Chakraborty, A. Mirizzi, N. Saviano and D. de Sousa Seixas, Phys. Rev. D **89**, 093001 (2014) [arXiv:1402.1767].
 - [21] I. Tamborra, F. Hanke, H.-T. Janka, B. Müller, G. G. Raffelt and A. Marek, Astrophys. J. **792**, 96 (2014) [arXiv:1402.5418].
 - [22] I. Tamborra, G. Raffelt, F. Hanke, H.-T. Janka and B. Müller, Phys. Rev. D **90**, 045032 (2014) [arXiv:1406.0006].
 - [23] E. Müller, H.-T. Janka and A. Wongwathanarat, Astron. Astrophys. **537**, 63 (2012) [arXiv:1106.6301].
 - [24] S. Hannestad, G. G. Raffelt, G. Sigl and Y. Y. Y. Wong, Phys. Rev. D **74**, 105010 (2006); Erratum *ibid.* **76**, 029901 (2007) [astro-ph/0608695].
 - [25] H. Duan, G. M. Fuller, J. Carlson and Y. Z. Qian, Phys. Rev. D **75**, 125005 (2007) [astro-ph/0703776].
 - [26] G. G. Raffelt and G. Sigl, Phys. Rev. D **75**, 083002 (2007) [hep-ph/0701182].
 - [27] A. Esteban-Pretel, S. Pastor, R. Tomàs, G. G. Raffelt and G. Sigl, Phys. Rev. D **76**, 125018 (2007) [arXiv:0706.2498].
 - [28] J. F. Cherry, J. Carlson, A. Friedland, G. M. Fuller and A. Vlasenko, Phys. Rev. Lett. **108**, 261104 (2012) [arXiv:1203.1607].
 - [29] J. F. Cherry, J. Carlson, A. Friedland, G. M. Fuller and A. Vlasenko, Phys. Rev. D **87**, 085037 (2013) [arXiv:1302.1159].
 - [30] S. Sarikas, I. Tamborra, G. Raffelt, L. Hudepohl and H.-T. Janka, Phys. Rev. D **85**, 113007 (2012) [arXiv:1204.0971].
 - [31] G. Mangano, A. Mirizzi and N. Saviano, Phys. Rev. D **89**, 073017 (2014) [arXiv:1403.1892].
 - [32] A. de Gouvea and S. Shalgar, JCAP **1210**, 027 (2012) [arXiv:1207.0516].
 - [33] A. de Gouvea and S. Shalgar, JCAP **1304**, 018 (2013) [arXiv:1301.5637].
 - [34] A. Vlasenko, G. M. Fuller and V. Cirigliano, Phys. Rev. D **89**, 105004 (2014) [arXiv:1309.2628].
 - [35] V. Cirigliano, G. M. Fuller and A. Vlasenko, arXiv:1406.5558.
 - [36] A. Vlasenko, G. M. Fuller and V. Cirigliano, arXiv:1406.6724.
 - [37] C. Volpe, D. Väänänen and C. Espinoza, Phys. Rev. D **87**, 113010 (2013) [arXiv:1302.2374].
 - [38] D. Väänänen and C. Volpe, Phys. Rev. D **88**, 065003 (2013) [arXiv:1306.6372].
 - [39] J. Serreau and C. Volpe, arXiv:1409.3591.
 - [40] E. Akhmedov, J. Kopp and M. Lindner, arXiv:1405.7275.
 - [41] A. Mirizzi and P. D. Serpico, Phys. Rev. D **86**, 085010 (2012) [arXiv:1208.0157].

- [42] A. Marek and H.-T. Janka, *Astrophys. J.* **694**, 664 (2009) [arXiv:0708.3372].
- [43] B. Müller, H.-T. Janka and A. Marek, *Astrophys. J.* **766**, 43 (2013) [arXiv:1210.6984].
- [44] H.-T. Janka, F. Hanke, L. Hüdepohl, A. Marek, B. Müller and M. Obergaulinger, *PTEP* **2012**, 01A309 (2012) [arXiv:1211.1378].